**PROBING ROCK TYPE, IRON REDOX STATE, AND TRANSITION METAL CONTENTS WITH SIX-WINDOW VNIR SPECTROSCOPY UNDER VENUS CONDITIONS.** M. D. Dyar[1], J. Helbert[2], T. Boucher[3], D. Wendler[2], I. Walter[4], T. Widemann[5], E. Marcq[6], A. Maturilli[2], S. Ferrari[7],1, M. D'Amore[2], N. Müller[8], and S. Smrekar[8], [1]Planet. Sci. Inst., 1700 East Fort Lowell, Tucson, AZ 85719 USA (mdyar@mtholyoke.edu); [2]Inst. Planet. Res., DLR, Rutherfordstrasse 2, 12489 Berlin, Germany; [3]Col. of Inform. and Computer Sci., Univ. of Massachusetts Amherst, Amherst, MA, 01003, USA; [4]Inst. Optical Sensorsystems, DLR, Rutherfordstrasse 2, 12489 Berlin, Germany, [5]LESIA; [6]LATMOS; [7]Dept. of Earth and Environmental Sciences, Univ. of Pavia, Via Ferrata 1 - 27100 Pavia, Italy; [8]Jet Propulsion Laboratory, California Institute of Technology, 4800 Oak Grove Dr., Pasadena CA, 91109.

Introduction: Although orbital VNIR spectroscopy of Venus is hampered by the presence of its thick, CO_2-rich atmosphere, recent experience shows that observations are possible through transparent windows in the CO_2 spectrum near 1 μm (**Figure 1**). Ground observers have successfully used these windows during the flyby of the Galileo mission at Jupiter [2]. The VIRTIS instrument on the ESA mission Venus Express (VEX) was the first instrument to routinely map the surface of Venus using the near-infrared windows from orbit [3-6]. The Venus Emissivity Mapper (VEM) was developed for the VERITAS mission to study the surface of Venus through six different windows at 0.86, 0.91, 0.99, 1.02, 1.11, and 1.18 μm. This project explores the rich scientific insights that can be gained using those six windows. Two specific issues are addressed here: the ability of VEM-window data to distinguish among key rock types on Venus, and the capability of VEM-window data to evaluate redox state and transition metal contents of Venus surface rocks.
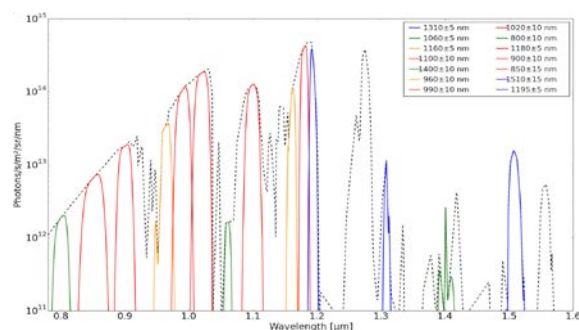
Figure 1. Highlands (red) and lowlands (blue) surface radiance spectra of Venus, with VEM filter locations superimposed [1].

Data: This project uses VNIR data collected in the Planetary Spectroscopy Laboratory (PSL) at the German Aerospace Center DLR in Berlin under the direction of Jörn Helbert [8-13]. Samples studied include a basalt from Lanzarote Island, Spain; a weathered basalt/basaltic andesite from Holyoke, Massachusetts; an amphibolite sample from Labrador (Canada); a trachybasalt from PEL collections (locality unknown); rhyolites from Lofoten Islands, Norway, and Seiser Alm, Italy; and rhyolitic glass from Newberry Volcano in Oregon (USA). Compositions were determined by x-

ray fluorescence (XRF) as described in [14] or by EMPA using standard methods. Fe^{3+}/Fe^{2+} ratios were measured using Mössbauer spectroscopy in the Mineral Spectroscopy Laboratory at Mount Holyoke College [15] using standard methods.
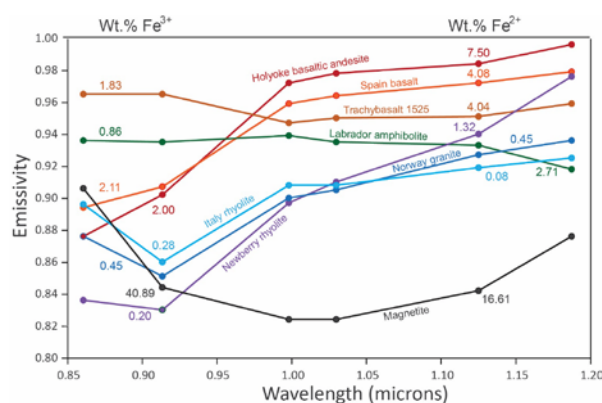
**Figure 2.** Emissivity data from PEL with wt. Fe^{2+} and wt.% Fe^{3+} indicated as determined by combining Mössbauer and EMPA data.

Assessing redox state and transition metal contents: The region of the visible spectrum where the CO_2 windows occur conveniently lies in a critical spectral region between most Fe^{3+} and Fe^{2+} features in silicates. Mössbauer data on the samples studied were used to convert the total Fe contents into wt% Fe^{3+} and wt% Fe^{2+}. These values are shown with the laboratory data in **Figure 2** below. Two trends are apparent. First, emissivities measured at the higher bands at 0.99, 1.02, 1.11, and 1.18 μm are indicative of the transition metal contents of the rocks, except for the amphibolite. This stems from the presence of Fe^{2+} and other transition metal absorptions near this spectral region. Further analysis of these data is needed to incorporate all the transition metals that may contribute to this spectral region.

Second, the wavelength region below 0.91 μm is related to the oxidation state of Fe in the rocks. The Fe oxide, magnetite, which is 67% Fe^{3+}, has the largest negative slope of any sample measured. Oxidized basalt/basaltic andesite and all the felsic rocks also have negative slopes, while the fresh basalts can be clearly distinguished on the basis of their positive slopes.

Based on these initial laboratory data, an oxidation state metric can easily be developed to distinguish among various Venus rock types.

Discriminating among rock types: Beyond simply determining chemical characteristics as discussed above, a key capability needed for understanding Venus is distinguishing between basalt plains on Venus
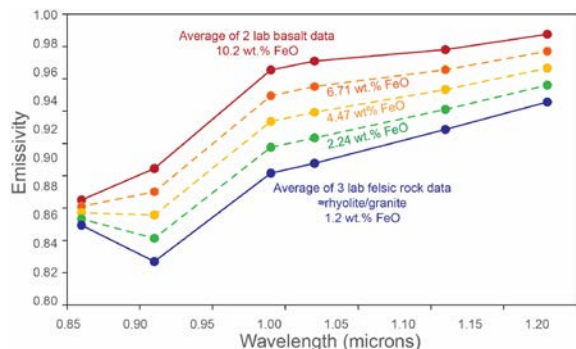
Figure 3. Spectra of synthetic rock types given as dashed lines between real average lab data, representing intermediate igneous rock types including basaltic andesite (6.71 wt.% FeO), andesite (4.47 wt.% FeO), and dacite (2.24 wt.% FeO). These FeO values were interpolated between the real average rock FeO compositions of samples run in the laboratory at DLR.

and other various igneous rock types (specifically basaltic andesite, andesite, dacite, and high SiO_2 rock types such as rhyolites and granites). To assess this issue, we used averages of our lab data (from Figure 2) and interpolated between them using FeO contents to obtain the model spectra for basaltic andesite, andesite, and dacite shown in **Figure 3**. We repeated these analyses using two different levels of error: the 4% VERITAS requirement and the currrent best estimates of errors following Phase A analyses. The values used for the latter were 0.7%, 0.7%, 0.4%, 0.3%, 0.7%, and 1.2% for the 0.86, 0.91, 0.99, 1.02, 1.11, and 1.18 µm bands, respectively. In each case, we then created 100 synthetic spectra within a random distribution of those errors.

Figure 4. Parameterization of the information in the six emissivity bands collected by VEM into 36 values that contain predictive information, of which 21 are independent. The 36 values are then used in models to discriminate among rock types.

For the 4% error spectra, we also parameterized each of the spectra by calculating the slope between each pair of band (15 combinations) as well as the band ratios between each pair of bands (again, 15 possibilities). This provided a total of 36 associated with each 4% error model (**Figure 4**). This full parameterization step was not necessary for the CBE spectra because 100% accuracy in classification was achieved using only the six channels of emissivity data (**Table 1**).

Next, we created a binary classifier to assess how accurately each of intermediate rock type could be distinguished from the basaltic plains of Venus. We used a regularized maximum entropy classifier, beginning by randomly holding out 20% of the data while the other 80% were used to train the model. The model was then used to predict the classification of the remaining 20%. We repeated 100 randomized trials for each model, with results shown in Table 1.

Table 1. Accuracy of Binary Classifier Trained to Distinguish between Rock Types

	n		Basalt / felsic	Basalt /dacite	Basalt / andesite	Basalt / BA
CBE errors	6	$\bar{x}$	100.0	100.0	100.0	100.0
		s^2	0.0	0.0	0.0	0.0
4% errors	36	$\bar{x}$	94.6	88.5	80.4	65.4
		s^2	0.6	0.9	1	1.2
	6	$\bar{x}$	93.7	86.4	80.2	60.1
		s^2	0.6	0.9	0.9	1.3

n = number of components in model, $\bar{x}$ = mean and s^2 = standard deviation of 100 trials. CBE errors as given in text.

This analysis shows that the highest accuracy in discriminating binary rock types is found (unsurprisingly) between mafic and felsic rocks. The most difficult distinction is between baslt and its closest compositional neighbor, basaltic andesite. However, basalt spectra can easily be distinguished from basaltic andesite at CBE error levels.

References: [1] Helbert J. et al. (2013) *IR Remote Sens. Instrum. XXI*, 8867, doi: 10.1117/12.2025582. [2] Carlson R. W. et al. (1991) *Science*, *253*, 1541-1548. [3] Mueller N. et al. (2008) *JGR 113*, 1–21. [4] Helbert J. et al. (2008) *GRL*, *35*, L11201. [5] Hashimoto G. L. et al. (2008) *JGR*, *113*, E00B24. [6] Piccioni G. et al. (2007) *ESA Special Pub.* 1295. [7] Helbert J. et al. (2013) *EPSL*, *369-370*, 233-238. [8] Maturilli A. and Helbert, J. (2006), *PSS*, *54*, 1057-1064. [9] Maturilli A. et al. (2008) *PSS*, *56*, 420-425. [10] Helbert J. and Maturilli A. (2009) *EPSL*, *285*, 347-354. [11] Maturilli A. and Helbert J. (2014) *J. Appl. Remote Sens.*, *8*, 084985. [12] Maturilli A. et al. (2014) *EPSL*, *398*, 58-65. [13] Maturilli et al. (2016) *LPS XLVIII,* Abstract #1402. [14] reference to wherever the compositional data are reported. [15] Dyar M. D. et al. (2016) *LPS XLVIII,* Abstract #2205.